Article

A Current Spectrum-Based Algorithm for Fault Detection of Electrical Machines Using Low-Power Data Acquisition Devices

Bilal Asad [1,2,*], Hadi Ashraf Raja [2], Toomas Vaimann [2], Ants Kallaste [2], Raimondas Pomarnacki [3] and Van Khang Hyunh [4]

1 Department of Electrical Power Engineering, The Islamia University of Bahawalpur, Bahawalpur 63100, Pakistan
2 Department of Electrical Power Engineering and Mechatronics, Tallinn University of Technology, 12616 Tallinn, Estonia; hadi.raja@taltech.ee (H.A.R.); toomas.vaimann@taltech.ee (T.V.); ants.kallaste@taltech.ee (A.K.)
3 Department of Electronic Systems, Vilnius Gediminas Technical University, 10223 Vilnius, Lithuania; raimondas.pomarnacki@vilniustech.lt
4 Department of Engineering Sciences, University of Agder, 4879 Grimstad, Norway; huynh.khang@uia.no
* Correspondence: bilal.asad@taltech.ee

Abstract: An algorithm to improve the resolution of the frequency spectrum by detecting the number of complete cycles, removing any fractional components of the signal, signal discontinuities, and interpolating the signal for fault diagnostics of electrical machines using low-power data acquisition cards is proposed in this paper. Smart sensor-based low-power data acquisition and processing devices such as Arduino cards are becoming common due to the growing trend of the Internet of Things (IoT), cloud computation, and other Industry 4.0 standards. For predictive maintenance, the fault representing frequencies at the incipient stage are very difficult to detect due to their small amplitude and the leakage of powerful frequency components into other parts of the spectrum. For this purpose, offline advanced signal processing techniques are used that cannot be performed in small signal processing devices due to the required computational time, complexity, and memory. Hence, in this paper, an algorithm is proposed that can improve the spectrum resolution without complex advanced signal processing techniques and is suitable for low-power signal processing devices. The results both from the simulation and practical environment are presented.

Keywords: electrical machine; machine learning; data acquisition; FEM; signal processing; Arduino; artificial intelligence

1. Introduction

The research in the predictive maintenance of electrical machines is touching new horizons. Cloud computation and distributed low-cost sensors are integral for Industry 4.0 standards. They can also be considered a paradigm shift in the predictive maintenance of electrical machines. Low-cost data acquisition sensors are becoming essential as electrical machines are becoming increasingly popular in small and medium-range electric vehicles. The research in the field of condition monitoring of electrical machines using stator currents [1–3], stator voltages [4–6], speed and torque ripples [7,8], stray flux [9–14], vibration analysis [15–19], thermal analysis [20–23], acoustic analysis [24–27], work in the steady-state interval [28], or transient regime [9,29–32] can be considered as mature enough after over a century of research. The research path started with conventional signal processing and harmonic estimation-based techniques. Here, the fundamental rule was to discover the fault-based new frequency components in the machine's global signal. The signal processing techniques were explored by researchers extensively to secure or protect the tiny, sensitive, fragile, and load-dependent fault-based information. For this purpose, the improvement in the spectrum resolution both in stationary and transient

regimes was the common point of interest. To remove the spectral leakage, the best practice both in IEEE and industry standards is to obtain the coherent sampling to the maximum extent [33,34]. A variety of other methods have also been explored in the literature, such as filter banks [35], adaptive filters [36,37], 2D feature [38], optimization of truncating windows [39,40], singular value decomposition [41–43], orthogonal matching pursuit [44–46], interpolated DFT techniques [47], Taylor Fourier transforms [48], multiple signal classification (MUSIC) [49,50], fault estimation using weighted iterative learning [51], auxiliary classifier generative adversarial network [52], and estimation of signal parameters via rotational invariance technique (ESPIRIT) [53]. The complexity of the required memory and calculation time are, however, problems that can limit their application in low-power data processing devices. The next major research domain is the mathematical modelling of electrical machines, as those are essential for the design, control, analysis, and fault-based simulations of electrical machines. The main task on which researchers put a lot of focus is to reduce the approximations and the simulation time of the fault simulation-compatible mathematical models. A large amount of research can be found in literature, ranging from finite element method (FEM) [54] to analytical models such as modified winding function analysis (MWFA) [55–57], reluctance network-based [58], and hybrid models [59,60]. As these models should be detailed and able to simulate every kind of fault, the simulation time and complexity are a big issue. The extended simulation time for fault diagnostics is not acceptable, as in the most advanced diagnostic techniques the simulation should run in parallel with the actual hardware, such as digital twin and hardware in the loop. A considerable research effort regarding the minimization of the simulation time both in FEM and analytical techniques can be found in literature, where [61] used piece-wise polynomial function for model order reduction, [62] used Loewner matrix interpolation, [63,64] used proper orthogonal decomposition, [65] used Krylov subspace techniques, etc. The development of these models opened new research directions where they can be used in the hardware in the loop environment [66], parameters estimation [67,68], digital twin [69], and inverse problem theory [70]. The research in these domains is complicated though due to the complex mathematical models, coupling effects in the motor variables, multiple solution points of the same problem, etc. These problems then opened the field, such as optimization theory [71], probability and stochastic analysis [72], non-linear control theory [73], and statistical analysis [74] of the global signals for the predictive maintenance of electrical machines. The development of these models paved the way towards another more advanced field, artificial intelligence [75]. A significant number of AI-based research articles can be seen in the literature and the number is increasing by leaps and bounds. The accuracy and maturity of AI algorithms depends on the data size and its variety under different loading and faulty conditions. Thanks to the research in the field of mathematical modelling, data collection under different faulty and loading conditions for a variety of different machines is possible using simulations. Moreover, data storage on the cloud can increase the training data set every day. The common point in all conventional and advanced techniques is the input signal. Mostly, the global signals remain the same for all types of machines as the state variables of all machines are almost the same. Now there is a paradigm shift in the measurement of all those signals using low-cost data acquisition devices such as Arduino cards and sending the data in the database without loss or any additional infiltrations such as noise.

In this paper, an algorithm is proposed that can improve the spectral resolution with the help of the following contributions.

1. The integral number of cycles and the signal's length whose prime factors are appropriate are calculated first. The fractional parts of the signal in the start and end reduce the spectrum's resolution, and an inappropriate length of the signal with a large number or size of prime factors decreases FFT's efficiency by increasing the complexity, required memory, and calculation time.
2. The low sampling frequency is the main problem when the data acquisition devices are not very powerful and are intended to work online with systems such as Arduino.

In Industry 4.0, those low-cost devices can have significant importance because of Internet of Things (IoT), distributed smart sensors, and cloud computation. The low sampling frequency leads to poor frequency resolution and increased spectral leakage. The main reason for this is sharp changes in the acquired signal. Hence, those sharp changes are proposed to be removed using data interpolation. This step is also important when the diagnostic algorithms depend on the mathematical model of the system. The most accurate models are the finite element method (FEM), based which the computational complexity is always a challenge. By using data interpolation, only the minimum number of steps can be simulated, and the rest of the values can be approximated.

3. Detecting any data discontinuity and removing it. In low power smart sensors, the chances of data loss cannot be neglected. This data loss can happen during its transmission from card to cloud due to network issues, due to some clock issues in the data acquisition card itself, or due to limited memory to save the signal before its transmission. This data loss is fatal for FFT-based spectrum analysis. This is due to the resultant data discontinuities in the acquired signals. So, a method is devised to remove data discontinuity, if any.

4. Repeating the cycles for the improvement in the resolution with minimal discontinuity. The increased number of signal cycles lead to a better frequency resolution. As the current and voltage cycles of the electrical machines working under steady state regime are periodic, they can be repeated to increase the signal's length. This repetition of the signal should not be random, which can make the resolution worse. Hence, a technique is proposed to repeat the cycles before frequency analysis if necessary.

2. The Theoretical Background

Almost all kinds of faults modulate the machine's global variables with a particular set of frequencies. The number and the amplitude of those frequency components are a function of the fault type and severity. During the early stages of fault, these harmonics are tiny in amplitude and difficult to detect. They tend to hide themselves under the frequency lobe of the powerful neighboring frequency component. The strength of any diagnostic algorithm is determined from its ability to detect those harmonics at the early stage of the fault. For this purpose, the resolution of the frequency spectrum is of significant importance, which increases with the decrease in the spectral leakage of the powerful frequency components. To reduce the spectral leakage, a variety of advanced signal processing techniques are available in the literature, but at the cost of increased computational time and complexity. It makes those algorithms less suitable for low power signal processing and controller boards. For low power smart sensor-based data acquisition and processing devices, the following fundamental precautionary measures should be accounted for.

5. The signal frequency and sampling frequency must follow conditions of coherency. The perfect coherent data is very difficult to obtain because of measurement equipment limitations and noise. This non-coherency can be avoided by windowing techniques [76]. However, the clever selection of the window is very important to obtain a narrower main lobe with less leakage energy inside the lobes. So, specialized knowledge about the windowing function and its impact on the spectrum is needed to deal with the problems, which cannot be a very easy solution. The drawback of FFT is that any mismatch between the sampling frequency and signal frequency can cause spectral leakage.

6. The signal should have an integer number of cycles. The fractional parts of the signal in the start or end increase the spectral leakage and increase the requirement of windowing function. This approach will increase the efficiency of FFT, will reduce the dependency on windowing function, and will reduce spectral leakage, even if the signal is noisy or its frequency is near the Nyquist rate. The quality of the frequency spectrum can be checked by measuring the signal to noise ratio (SNR), total harmonic distortion (THD), spurious free dynamic range (SFDR), signal to noise and distortion

ratio (SNDR), effective number of bits (ENOF), etc. The number of cycles in a signal can be calculated as

$$J = M\frac{f_{in}}{f_s} = J_{int} + \Delta \tag{1}$$

In this equation, J is the total number of cycles, fin is the frequency of the fundamental component of the near sinusoid signal, f_s is the sampling frequency, M is the recorded signal's length, J_{int} are the integral number of signal cycles, and Δ is the fractional part. The non-zero Δ leads to the spectral leakage.

A signal from time domain to discrete domain can be represented as

$$x(t) = A sin(2\pi f_{in}t + \theta) + hh \tag{2}$$

$$x[k] = A sin\left(2\pi f_{in}\frac{k}{f_s} + \theta\right) + hh \tag{3}$$

$$x[k] = A sin\left(2\pi \frac{J}{M}k + \theta\right) + hh \tag{4}$$

$$x[k] = A sin\left(2\pi \frac{J_{int} + \Delta}{M}k + \theta\right) + hh \tag{5}$$

$$x[k] = x_1[k] + x_h[k] \tag{6}$$

where hh represents the higher order harmonics and can be defined as follows: a_n and b_n are the Fourier coefficients.

$$hh(t) = \sum_{n \geq 2}(a_n cos2\pi n f_{in}t + b_n sin2\pi n f_{in}t) \tag{7}$$

In squirrel cage induction machines, the main causes of these higher order harmonics are the non-sinusoidal winding distributions, changing airgap reluctance due to rotor and stator slot openings, inherent eccentricity, material saturation, harmonics coming from the supply, and any fault if present in the machine. However, all these harmonics are tiny in comparison with the fundamental component and the overall current signal remains near sinusoidal. The initial purpose is to calculate J_{int} in the acquired signal and discard the fractional part Δ.

The integer number of cycles are calculated in the way that all values greater than the RMS value both on positive and negative half cycle are marked as +1 and -1. All elements are merged into one if the adjacent sign is the same to make a new signal say w[m]. We merge adjacent same values into one element and take the absolute value.

3. The Effect of Discontinuities in the Signal

Although FFT is a very powerful tool that is extensively used in the field of signal processing, for smooth, periodic, uniformly sampled points and long signals, FFT no doubt gives accurate results. However, the results become significantly erroneous if there are singularities or discontinuities in the signals. Thanks to the symmetrical and sinusoidal distributed design and performance parameters of electrical machines, almost all global signals such as current, voltage, and flux are periodic. The data discontinuities are however possible due to the limitations of the data acquisition devices, particularly if those are low power cards. This can be because of network limitations such as delay or loss of data transfer from the device to cloud. Because of the high sample rate, there is a high chance of data loss while data is being transferred from sensors to the low power cards. This is mostly because of the delay in the clearance of the buffers when data are being transmitted for a long time, i.e., a couple of days to weeks. An example of such a data acquisition system is shown in Figure 1.
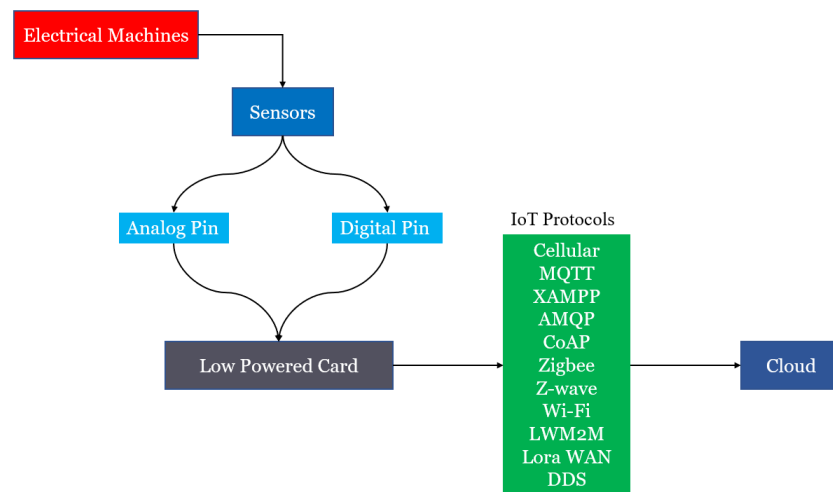
Figure 1. The schematic diagram of data acquisition and transmission to the cloud using IoT.

Data loss can occur in two scenarios for the above data acquisition setup, while the data are being transferred from sensors to the low powered cards and the other while the data are being transferred from the cards to cloud. The protocols used for data transmission have their own limitations too. The loss of data during transmission can be due to the limitation of network or delay/loss of network while transferring. Another reason might be due to the buffers being overloaded and not being properly cleared up before the next data come in, which can result in a loss of data while in transmission. These sharp changes in the signal are the potential cause of hiding the low power fault-based frequencies due to the increased spectral leakage of significant harmonics. It also decreases the computational time of FFT, decreases its efficiency, and increases the need for increased data length. The experimental setup used to recreate such scenario is shown in Figure 2.
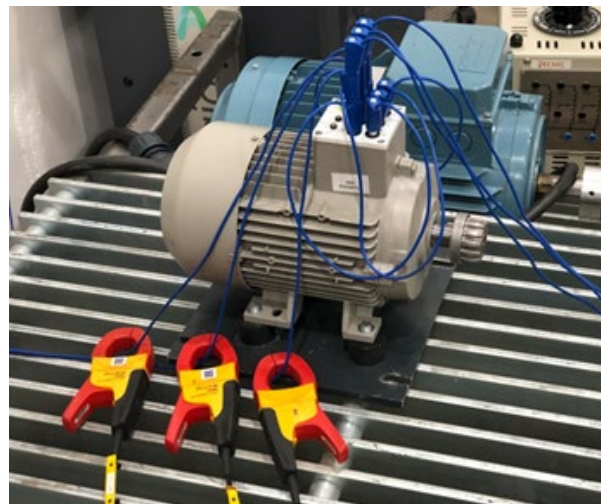

Figure 2. Experimental setup for data collection.

The induction motor is used to collect current signals for all three phases, and it is then transmitted to the cloud using Arduino (low powered card). This is the most common approach used for the data acquisition system when using a low powered card. There are alternate systems that have been proposed that further consider data losses with a local backup of collected data at a node [ref], but the following approach is still widely used. The flow chart of the setup used for data collection for this experiment is shown in Figure 3.
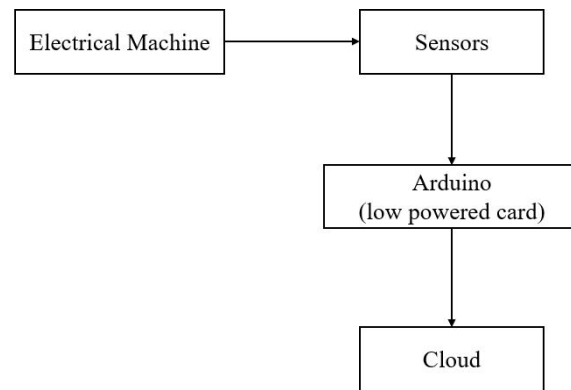
Figure 3. Flow chart for the data acquisition setup.

The setup was run continuously for multiple days with different sampling rates to generate data losses. At higher sampling rates, the data losses occurred more often as the buffer became overloaded. Because of the limitation of the processing power of Arduino (low powered cards), data loss became inevitable in these cases. This is why the sampling rate tended to be on the lower side in most cases, but this also resulted in the samples being too low and similar data loss issues could occur if it kept running for a more extended period. The other scenario was also created by interrupting the network connection. In this case, wi-fi was used to transmit data from Arduino to the cloud database. Upon interruption of the network, as no data were transmitted, this resulted in data being lost. For some protocols, it could result in a delay at the receiving end, but this will still have components lost for the received signal. The setup was used to obtain signals with data discontinuity to check the result of the proposed algorithm.

The data discontinuities were detected by making a moving subtraction filter. The amplitude difference of every two consecutive samples defined the magnitude of discontinuity in them. For example, in Figure 4, nine discontinuities along with their amplitude are discovered that need correction.
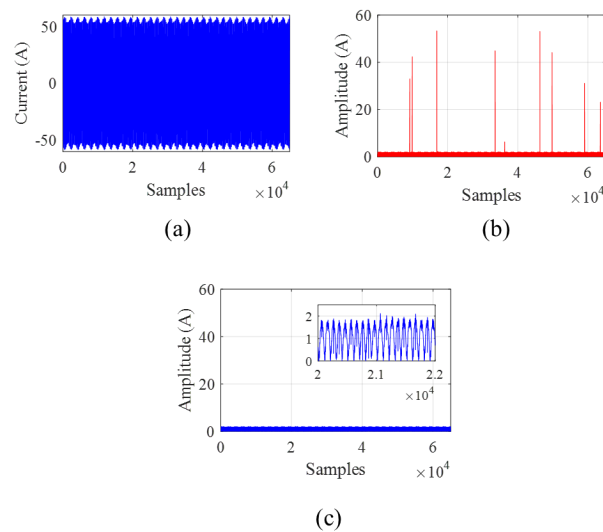
$$diff = |x[n]| - |x[n-1]| \tag{8}$$

Figure 4. (**a**) The acquired stator current, (**b**) the result of moving subtraction filter for the detection of discontinuities, and (**c**) after the correction of discontinuous samples.

For correction, the discontinuous sample is replaced with the average value of the samples $x[n-1]$ and $x[n+1]$:

$$\hat{x}[n] = \frac{|x[n+1]| + |x[n-1]|}{2} \qquad (9)$$

The integer number of cycles can be calculated using zero cross detection, but, in that case, wrong computation can occur if there is any data discontinuity in the signal. If there are more than one consecutive missing data samples then there are some possible methods of correction. Replace the missing samples with the samples from the same location of the subsequent cycle. The other way is that the samples will be replaced by random values, depending on the amplitude of the available samples at the start and end of the missing segment and the amplitude will be iteratively corrected. The third way is that if the cycles are affected in a worse manner, then it can be totally replaced with the healthy one from the signal. This paper at the moment deals with only one discontinuity between two healthy samples.

4. Counting the Integral Number of Cycles and Removing the Fractional Parts

The integral number of cycles are calculated in the following steps.

A.　The samples of the acquired stator current are compared with the RMS value. The samples with a magnitude greater than the RMS value for both the positive and negative side are replaced with one, while all of the other samples are replaced with zero as shown in the equation below and Figure 5b.

$$y[k] = \begin{cases} 1, \frac{i_m}{\sqrt{2}} \le i[k] \\ 0, \frac{i_m}{\sqrt{2}} \ge |i[k]| \\ -1, -\frac{i_m}{\sqrt{2}} \ge i[k] \end{cases} \qquad (10)$$
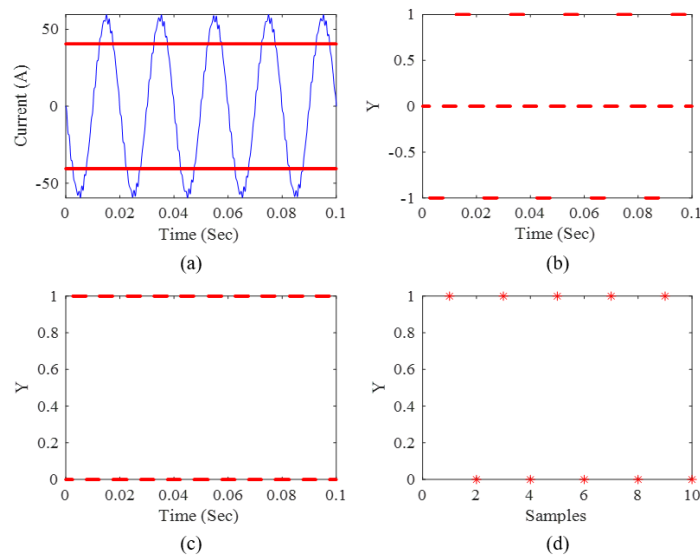

Figure 5. (**a**) The stator current with red line representing the RMS value, (**b**) the samples validating the conditions given in b, (**c**) the shifting of negative samples towards positive side by taking modulus, and (**d**) merging the consecutive samples of same value in one.

B.　The modulus of the resultant vector is taken to shift the negative-sided samples to the positive side, as shown in Figure 5c.

C.　The consecutive samples with same magnitude are merged into one and represented in Figure 5d. The final number of samples on the zero or unity axis are equal to the number of signal cycles.

After counting the number of cycles, the data are saved until the index of steric completing the integral number of cycles in Figure 5d. Now, two types of discontinuities may still persist in the signal: the minor discontinuity due to low sampling frequency, as shown in Figure 6, and the possible discontinuity at te starting and ending time.
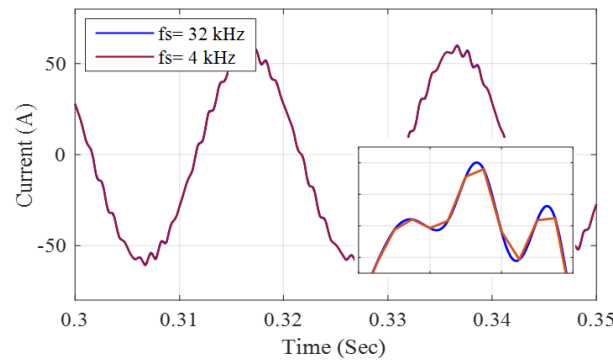

Figure 6. The estimation of intermediate solutions using data interpolation.

Both problems can be solved by signal interpolation. It will not only improve the smoothness of the signal, but also refine the zero crossing points, as shown in Figure 7.
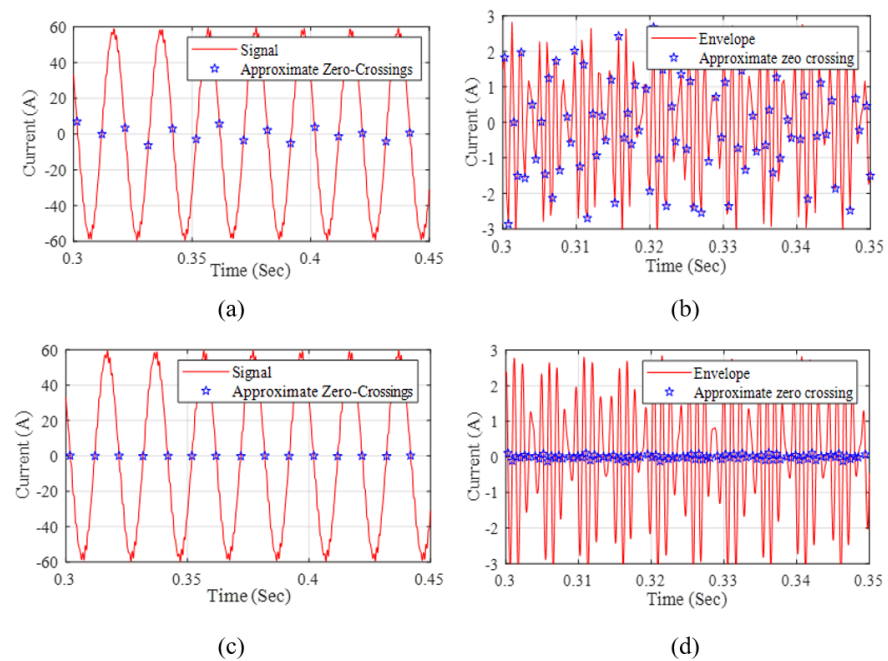

Figure 7. (**a**) The stator current and approximate zero crossings at a sampling frequency of 4 kHz, (**b**) the corresponding envelope shifted across zero line with approximate zero crossings, (**c**) the signal with improved sampling frequency and approximate zero crossings, and (**d**) the corresponding envelope shifted across zero line with approximate zero crossings.

5. Algorithm

The proposed algorithm is shown in Figure 8. Its main parts include the removal of DC offset which decreases the possibility of a frequency bin at 0Hz in the spectrum, detection and correction of data discontinuities which increase the spectral leakage, removal of starting and ending fractional parts and the repetition of the signal if necessary.
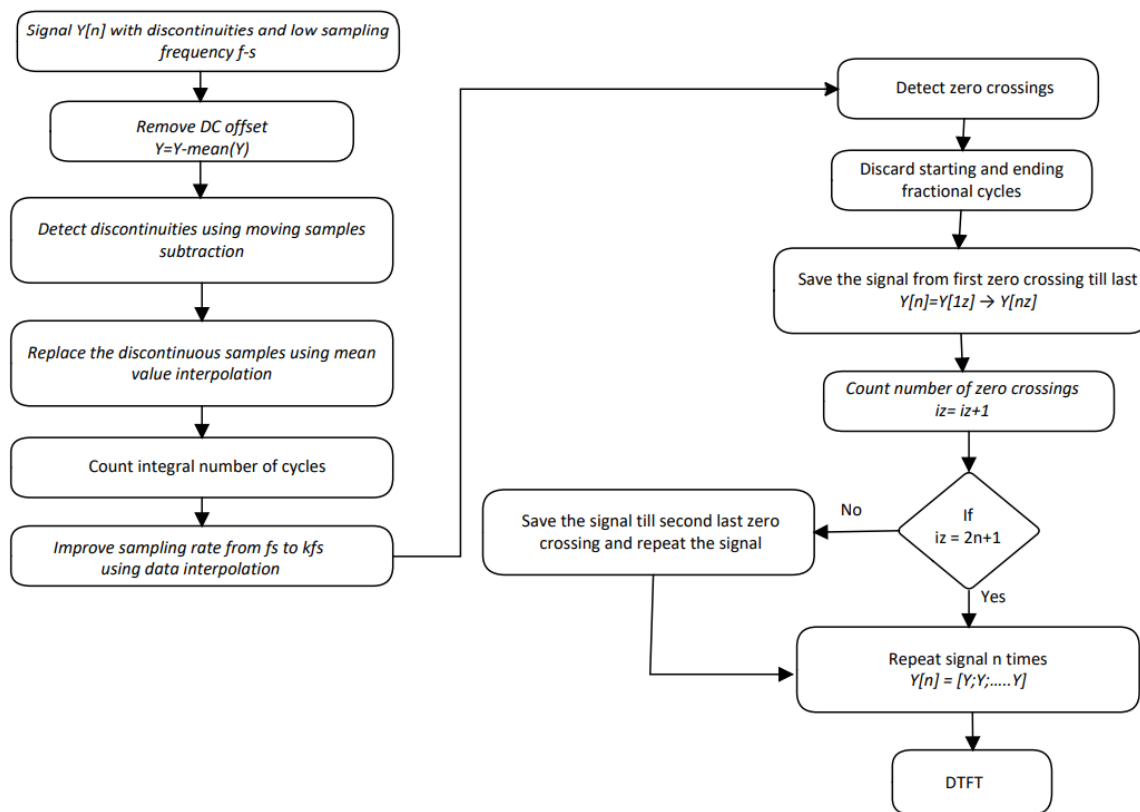
Figure 8. The algorithm for counting the integral number of cycles, removal of signal discontinuities and fractional parts of the signal, data interpolation, and repetition, if necessary.

6. Results

6.1. Simulation Results

The motor's stator current harmonics can be broadly classified into three major categories: the winding and supply-based odd multiples of the fundamental component, the slotting harmonics, and the fault generated harmonics. The mathematical description of these harmonics is given in Table 1. The fault and slotting harmonics are the function of slip and tend to move in the spectrum as the load varies, while the winding MMF and the supply harmonics retain their position in the spectrum. Electrical machine simulations are necessary for several reasons, such as design, control, analysis, and training of the fault diagnostic algorithms, creation of digital twin, inverse problem theory, hardware in the loop environment, and parameters estimation. However, the biggest drawback of finite element method (FEM) models of electrical machines is the computational complexity and the required simulation time. Moreover, the small step size and the simulation of complete geometry is required for better resolution of the spectrum because for predictive maintenance, the importance of wideband harmonics cannot be denied. For this purpose, the algorithm is first implemented on FEM-based simulation signals with a low sampling frequency. In Figure 9, it can be seen that even at a high step size with a sampling frequency of 4 kHz, the spectrum counting the integral number of cycles increases the resolution significantly without the need for any truncating window. Moreover, the effect of communication channel-based data discontinuities and their correction is shown in Figure 10.

Table 1. Fault definition frequencies.

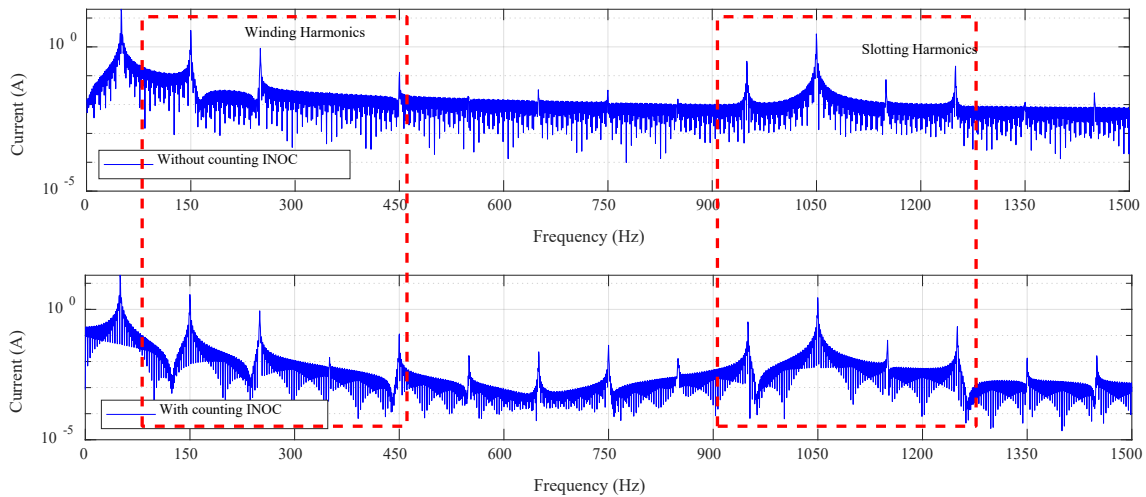| Fault	Modulating Frequencies
Broken Rotor Bars	$f_{BR} = f_s \pm 2ks f_s, \quad k = 1, 2, 3, \ldots$
Principal slotting harmonic (PSH) and Eccentricity	$f_{ecce} = \left[(kn_b \pm n_d) \left(\frac{1-s}{p} \right) \pm v \right] fs$ More precisely: $f_{ecce} = \left[1 \pm k \left(\frac{1-s}{p} \right) \right] fs$ $f_{ecce} = f_s \pm k f_r, \quad k = 1, 2, 3, \ldots$

Figure 9. The simulated stator current spectrum showing stator winding and slotting harmonics before and after counting integral number of cycles (INOC).
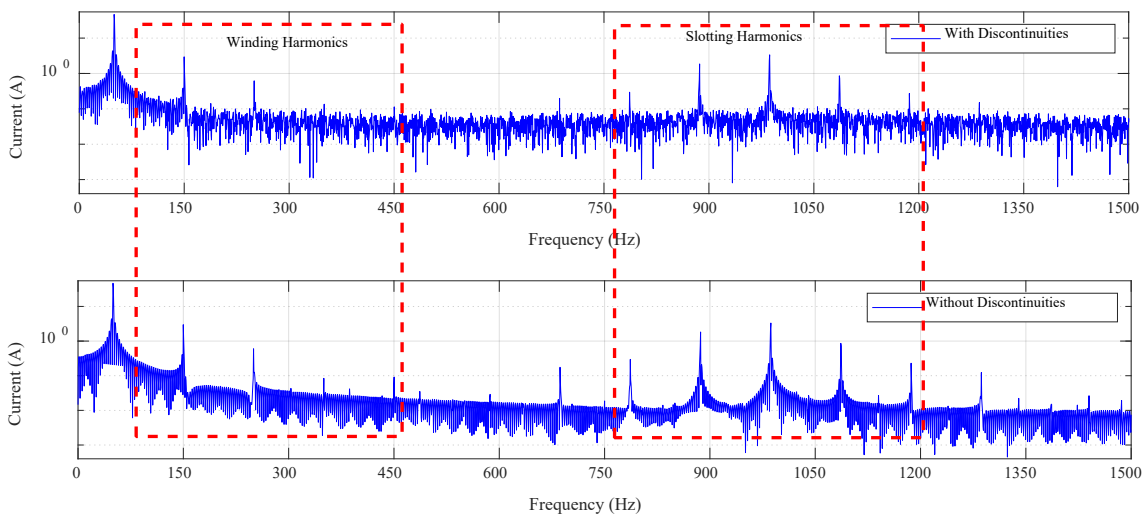

Figure 10. The effect of signal discontinuities on the spectrum resolution.

6.2. Practical Results

For practical investigations, two similar machines were connected back-to-back. One machine works as a loading machine, while the other was used as a testing motor where the healthy and broken rotor bar carrying rotor were tested. Table 2 shows the nominal parameters of the machine under investigation. Figures 11 and 12 show the improvement in the spectrum resolution by removing the fractional parts of the signal and data discontinuities without any truncating window. The tiny broken rotor bar harmonics near the strong supply and spatial harmonics became well legible.

Table 2. The machine specifications.

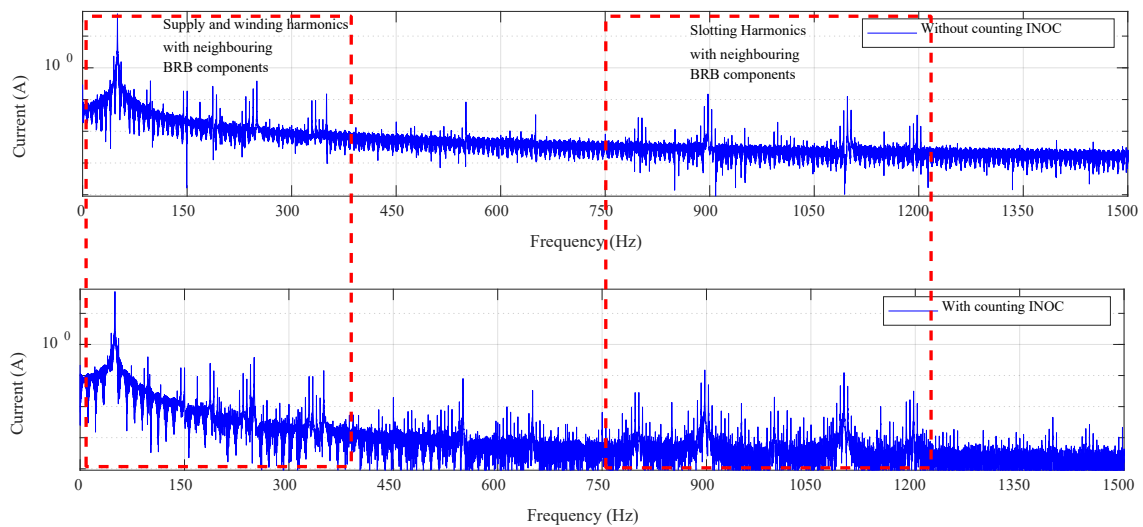| Parameter	Symbol	Value
Number of poles	P	4
Number of phases	φ	3
Connection	-	Star
Stator slots	Ns	48, non-skewed
Rotor bars	Nb	40, skewed
Rated voltage	V	333 V @50 Hz
Rated power	Pr	18 kW @50 Hz

Figure 11. The practical stator current spectrum showing stator winding, slotting, and broken rotor bar-based harmonics before and after counting the integral number of cycles (INOC).
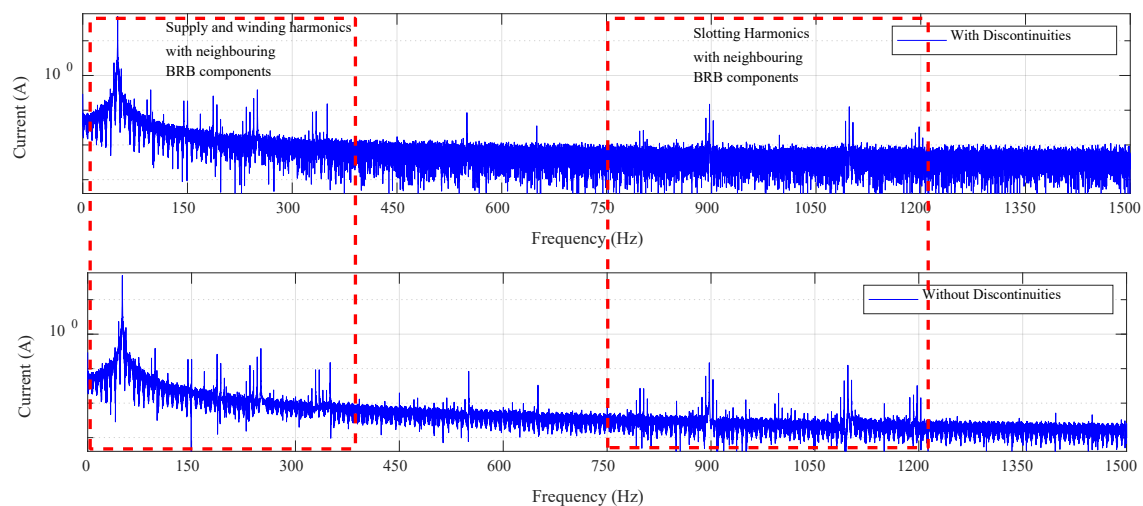

Figure 12. The practical stator current spectrum showing stator winding, slotting, and broken rotor bar-based harmonics with and without discontinuities.

The frequency of slotting harmonics in the current spectrum in comparison with their expected frequency according to the equations given in Table 1 as a function of slip is shown in Table 3. It is clear that the amplitude of those harmonics decreases with the decreasing slip, which makes their detection difficult when the machine is working under low or no-load conditions.

Table 3. The rotor slot harmonics (RSH).

Slip	Theoretical RSH1	Theoretical RSH2	RSH1 (Hz)	RSH2 (Hz)	RSH1 (A)	RSH2 (A)
0.0030	947	1047	946.7	1046.8	0.00042	0.0005
0.035	915	1015	914.76	1014.76	0.00185	0.0008
0.05	900	1000	899.2	999.2	0.0021	0.0007

7. Conclusions

Low sampling frequency, fractional parts of the signal at starting and ending, and data discontinuities in the time domain can lead to spectral leakage in the frequency domain when applying the FFT (Fast Fourier Transform) algorithm. Spectral leakage refers to the effect where energy from a signal at one frequency "leaks" into other nearby frequencies, creating artifacts in the spectrum that are not present in the original signal. There can also be interruptions between the transmitted signals due to limitations of the hardware used or because of a loss of network. This can also lead to data loss or the receiving signal missing some harmonics and having some junk values in between. This can further lead to an incorrect analysis of the collected signal, and, in some cases, it might even be more fatal, i.e., could lead to the machine being damaged if the issue occurs in the case of monitoring an electrical machine.

One way to mitigate these effects is by applying a window function to the data before performing the FFT. A window function can smooth out the signal at the edges of the analysis window, reducing the abrupt changes and thus the spectral leakage. However, even with a window function, some level of spectral leakage may still be present, depending on the characteristics of the signal and the choice of window function. Moreover, the application of advanced signal processing techniques makes it computationally complex for low power data acquisition and processing devices.

This paper shows how a simple algorithm can improve the spectrum resolution by removing the above-mentioned problems.

Author Contributions: Conceptualization, B.A., H.A.R. and T.V.; methodology, B.A. and H.A.R.; software, B.A. and H.A.R.; validation, T.V., A.K. and R.P.; formal analysis, V.K.H.; investigation, B.A.; resources, T.V.; data curation, B.A.; writing—original draft preparation, B.A. and H.A.R.; writing—review and editing, T.V.; visualization, A.K.; supervision, V.K.H.; project administration, V.K.H. and T.V.; funding acquisition, T.V. and V.K.H. All authors have read and agreed to the published version of the manuscript.

Institutional Review Board Statement: Not applicable.

Informed Consent Statement: Not applicable.

Data Availability Statement: The data presented in this study are available within the article.

References

1. Skarmoutsos, G.A.; Gyftakis, K.N.; Mueller, A.M. Analytical Prediction of the MCSA Signatures Under Dynamic Eccentricity in PM Machines with Concentrated Non-Overlapping Windings. *IEEE Trans. Energy Convers.* **2021**, *37*, 1011–1019. [CrossRef]
2. Garcia-Bracamonte, J.E.; Ramirez-Cortes, J.M.; de Jesus Rangel-Magdaleno, J.; Gomez-Gil, P.; Peregrina-Barreto, H.; Alarcon-Aquino, V. An Approach on MCSA-Based Fault Detection Using Independent Component Analysis and Neural Networks. *IEEE Trans. Instrum. Meas.* **2019**, *68*, 1353–1361. [CrossRef]

3. Asad, B.; Vaimann, T.; Belahcen, A.; Kallaste, A.; Rassõlkin, A.; Iqbal, M.N. Broken rotor bar fault detection of the grid and inverter-fed induction motor by effective attenuation of the fundamental component. *IET Electr. Power Appl.* **2019**, *13*, 2005–2014. [CrossRef]

4. Hang, J.; Hu, Q.; Sun, W.; Ren, X.; Ding, S.; Huang, Y.; Hua, W. A Voltage-Distortion-Based Method for Robust Detection and Location of Interturn Fault in Permanent Magnet Synchronous Machine. *IEEE Trans. Power Electron.* **2022**, *37*, 11174–11186. [CrossRef]

5. Hu, R.; Wang, J.; Mills, A.R.; Chong, E.; Sun, Z. High-Frequency Voltage Injection Based Stator Interturn Fault Detection in Permanent Magnet Machines. *IEEE Trans. Power Electron.* **2020**, *36*, 785–794. [CrossRef]

6. Irhoumah, M.; Pusca, R.; Lefevre, E.; Mercier, D.; Romary, R. Detection of the Stator Winding Inter-Turn Faults in Asynchronous and Synchronous Machines Through the Correlation Between Harmonics of the Voltage of Two Magnetic Flux Sensors. *IEEE Trans. Ind. Appl.* **2019**, *55*, 2682–2689. [CrossRef]

7. Yang, M.; Chai, N.; Liu, Z.; Ren, B.; Xu, D. Motor Speed Signature Analysis for Local Bearing Fault Detection with Noise Cancellation Based on Improved Drive Algorithm. *IEEE Trans. Ind. Electron.* **2019**, *67*, 4172–4182. [CrossRef]

8. Hu, K.; Liu, Z.; Tasiu, I.A.; Chen, T. Fault Diagnosis and Tolerance with Low Torque Ripple for Open-Switch Fault of IM Drives. *IEEE Trans. Transp. Electrif.* **2020**, *7*, 133–146. [CrossRef]

9. Tian, P.; Antonino-Daviu, J.A.; Platero, C.A.; Dunai, L.D. Detection of Field Winding Faults in Synchronous Motors via Analysis of Transient Stray Fluxes and Currents. *IEEE Trans. Energy Convers.* **2020**, *36*, 2330–2338. [CrossRef]

10. Gurusamy, V.; Baruti, K.H.; Zafarani, M.; Lee, W.; Akin, B. Effect of Magnets Asymmetry on Stray Magnetic Flux Based Bearing Damage Detection in PMSM. *IEEE Access* **2021**, *9*, 68849–68860. [CrossRef]

11. Filho, P.C.M.L.; Baccarini, L.M.R.; Batista, F.B.; Araujo, A.C. Orbit Analysis froma Stray Flux Full Spectrum for Induction Machine Fault Detection. *IEEE Sensors J.* **2021**, *21*, 16152–16161. [CrossRef]

12. Liu, X.; Miao, W.; Xu, Q.; Cao, L.; Liu, C.; Pong, P.W.T. Inter-Turn Short-Circuit Fault Detection Approach for Permanent Magnet Synchronous Machines Through Stray Magnetic Field Sensing. *IEEE Sensors J.* **2019**, *19*, 7884–7895. [CrossRef]

13. Gurusamy, V.; Bostanci, E.; Li, C.; Qi, Y.; Akin, B. A Stray Magnetic Flux-Based Robust Diagnosis Method for Detection and Location of Interturn Short Circuit Fault in PMSM. *IEEE Trans. Instrum. Meas.* **2020**, *70*, 6045–6057. [CrossRef]

14. Park, Y.; Choi, H.; Bin Lee, S.; Gyftakis, K.N. Search Coil-Based Detection of Nonadjacent Rotor Bar Damage in Squirrel Cage Induction Motors. *IEEE Trans. Ind. Appl.* **2020**, *56*, 4748–4757. [CrossRef]

15. Reda, K.; Yan, Y. Vibration Measurement of an Unbalanced Metallic Shaft Using Electrostatic Sensors. *IEEE Trans. Instrum. Meas.* **2018**, *68*, 1467–1476. [CrossRef]

16. Song, L.; Wang, H.; Chen, P. Vibration-Based Intelligent Fault Diagnosis for Roller Bearings in Low-Speed Rotating Machinery. *IEEE Trans. Instrum. Meas.* **2018**, *67*, 1887–1899. [CrossRef]

17. Samanta, A.K.; Routray, A.; Khare, S.R.; Naha, A. Minimum Distance-Based Detection of Incipient Induction Motor Faults Using Rayleigh Quotient Spectrum of Conditioned Vibration Signal. *IEEE Trans. Instrum. Meas.* **2021**, *70*, 1–11. [CrossRef]

18. Rafaq, M.S.; Lee, H.; Park, Y.; Bin Lee, S.; Fernandez, D.; Diaz-Reigosa, D.; Briz, F. A Simple Method for Identifying Mass Unbalance Using Vibration Measurement in Permanent Magnet Synchronous Motors. *IEEE Trans. Ind. Electron.* **2021**, *69*, 6441–6444. [CrossRef]

19. Kudelina, K.; Asad, B.; Vaimann, T.; Belahcen, A.; Rassõlkin, A.; Kallaste, A.; Lukichev, D.V. Bearing Fault Analysis of BLDC Motor for Electric Scooter Application. *Designs* **2020**, *4*, 42. [CrossRef]

20. Choudhary, A.; Goyal, D.; Letha, S.S. Infrared Thermography-Based Fault Diagnosis of Induction Motor Bearings Using Machine Learning. *IEEE Sensors J.* **2020**, *21*, 1727–1734. [CrossRef]

21. Mohammed, A.; Melecio, J.I.; Djurovic, S. Open-Circuit Fault Detection in Stranded PMSM Windings Using Embedded FBG Thermal Sensors. *IEEE Sensors J.* **2019**, *19*, 3358–3367. [CrossRef]

22. Shi, Y.; Wang, J.; Hu, R.; Wang, B. Electromagnetic and Thermal Behavior of a Triple Redundant 9-Phase PMASynRM with Insulation Deterioration Fault. *IEEE Trans. Ind. Appl.* **2020**, *56*, 6374–6383. [CrossRef]

23. Mohammed, A.; Melecio, J.I.; Djurovic, S. Stator Winding Fault Thermal Signature Monitoring and Analysis by In Situ FBG Sensors. *IEEE Trans. Ind. Electron.* **2018**, *66*, 8082–8092. [CrossRef]

24. Lucas, G.B.; de Castro, B.A.; Rocha, M.A.; Andreoli, A.L. A New Acoustic Emission-Based Approach for Supply Disturbances Evaluation in Three-Phase Induction Motors. *IEEE Trans. Instrum. Meas.* **2020**, *70*, 1–10. [CrossRef]

25. Parvathi Sangeetha, B.; Hemamalini, S. Rational-Dilation Wavelet Transform Based Torque Estimation from Acoustic Signals for Fault Diagnosis in a Three-Phase Induction Motor. *IEEE Trans. Ind. Inform.* **2018**, *15*, 3492–3501. [CrossRef]

26. Liu, F.; Wu, R.; Teng, F.; Liu, Y.; Lu, S.; Ju, B.; Cao, Z. A Two-Stage Learning Model for Track-Side Acoustic Bearing Fault Diagnosis. *IEEE Trans. Instrum. Meas.* **2021**, *70*, 1–12. [CrossRef]

27. Liu, Z.; Yang, B.; Wang, X.; Zhang, L. Acoustic Emission Analysis for Wind Turbine Blade Bearing Fault Detection Under Time-Varying Low-Speed and Heavy Blade Load Conditions. *IEEE Trans. Ind. Appl.* **2021**, *57*, 2791–2800. [CrossRef]

28. Sun, C.; Liu, W.; Han, X.; Zhang, X.; Jiao, N.; Mao, S.; Wang, R.; Guan, Y. High-Frequency Voltage Injection-Based Fault Detection of a Rotating Rectifier for a Wound-Rotor Synchronous Starter/Generator in the Stationary State. *IEEE Trans. Power Electron.* **2021**, *36*, 13423–13433. [CrossRef]

29. Zamudio-Ramirez, I.; Ramirez-Nunez, J.A.; Antonino-Daviu, J.; Osornio-Rios, R.A.; Quijano-Lopez, A.; Razik, H.; Romero-Troncoso, R.J. Automatic diagnosis of electromechanical faults in induction motors based on the transient analysis of the stray flux via MUSIC methods. *IEEE Trans. Ind. Appl.* **2020**, *56*, 3604–3613. [CrossRef]

30. Gyftakis, K.N. A Comparative Investigation of Interturn Faults in Induction Motors Suggesting a Novel Transient Diagnostic Method Based on the Goerges Phenomenon. *IEEE Trans. Ind. Appl.* **2021**, *58*, 304–313. [CrossRef]

31. Park, Y.; Choi, H.; Shin, J.; Park, J.; Bin Lee, S.; Jo, H. Airgap Flux Based Detection and Classification of Induction Motor Rotor and Load Defects During the Starting Transient. *IEEE Trans. Ind. Electron.* **2020**, *67*, 10075–10084. [CrossRef]

32. Asad, B.; Vaimann, T.; Belahcen, A.; Kallaste, A.; Rassõlkin, A.; Ghafarokhi, P.; Kudelina, K. Transient Modeling and Recovery of Non-Stationary Fault Signature for Condition Monitoring of Induction Motors. *Appl. Sci.* **2021**, *11*, 2806. [CrossRef]

33. *IEEE Std 1658-2011*; IEEE Standard for Terminology and Test Methods of Digital-to-Analog Converter Devices. IEEE: Pisataway, NJ, USA, 2012. [CrossRef]

34. *P1057^{TM}/D8*; IEEE Standard for Digitizing Waveform Recorders. IEEE: New York, NY, USA, 2018.

35. Li, R.; Zhuang, L.; Li, Y.; Shen, C. Intelligent Bearing Fault Diagnosis Based on Scaled Ramanujan Filter Banks in Noisy Environments. *IEEE Trans. Instrum. Meas.* **2021**, *70*, 1–13. [CrossRef]

36. Gao, M.; Yu, G.; Wang, T. Impulsive Gear Fault Diagnosis Using Adaptive Morlet Wavelet Filter Based on Alpha-Stable Distribution and Kurtogram. *IEEE Access* **2019**, *7*, 72283–72296. [CrossRef]

37. Atta, M.E.E.-D.; Ibrahim, D.K.; Gilany, M.I. Broken Bar Faults Detection Under Induction Motor Starting Conditions Using the Optimized Stockwell Transform and Adaptive Time–Frequency Filter. *IEEE Trans. Instrum. Meas.* **2021**, *70*, 1–10. [CrossRef]

38. Gong, W.; Chen, H.; Zhang, Z.; Zhang, M.; Gao, H. A Data-Driven-Based Fault Diagnosis Approach for Electrical Power DC-DC Inverter by Using Modified Convolutional Neural Network with Global Average Pooling and 2-D Feature Image. *IEEE Access* **2020**, *8*, 73677–73697. [CrossRef]

39. Hou, B.; Wang, D.; Chen, Y.; Wang, H.; Peng, Z.; Tsui, K.-L. Interpretable online updated weights: Optimized square envelope spectrum for machine condition monitoring and fault diagnosis. *Mech. Syst. Signal Process.* **2022**, *169*, 108779. [CrossRef]

40. Burriel-Valencia, J.; Puche-Panadero, R.; Martinez-Roman, J.; Sapena-Bano, A.; Pineda-Sanchez, M. Fault Diagnosis of Induction Machines in a Transient Regime Using Current Sensors with an Optimized Slepian Window. *Sensors* **2018**, *18*, 146. [CrossRef]

41. Cong, F.; Chen, J.; Dong, G.; Zhao, F. Short-time matrix series based singular value decomposition for rolling bearing fault diagnosis. *Mech. Syst. Signal Process.* **2013**, *34*, 218–230. [CrossRef]

42. Kang, M.; Kim, J.-M. Singular value decomposition based feature extraction approaches for classifying faults of induction motors. *Mech. Syst. Signal Process.* **2013**, *41*, 348–356. [CrossRef]

43. Li, H.; Liu, T.; Wu, X.; Chen, Q. A Bearing Fault Diagnosis Method Based on Enhanced Singular Value Decomposition. *IEEE Trans. Ind. Inform.* **2020**, *17*, 3220–3230. [CrossRef]

44. Yi, C.; Ran, L.; Tang, J.; Jin, H.; Zhuang, Z.; Zhou, Q.; Lin, J. An Improved Sparse Representation Based on Local Orthogonal Matching Pursuit for Bearing Compound Fault Diagnosis. *IEEE Sens. J.* **2022**, *22*, 21911–21923. [CrossRef]

45. Morales-Perez, C.; Rangel-Magdaleno, J.; Peregrina-Barreto, H.; Amezquita-Sanchez, J.P.; Valtierra-Rodriguez, M. Incipient Broken Rotor Bar Detection in Induction Motors Using Vibration Signals and the Orthogonal Matching Pursuit Algorithm. *IEEE Trans. Instrum. Meas.* **2018**, *67*, 2058–2068. [CrossRef]

46. Wang, L.; Cai, G.; You, W.; Huang, W.; Zhu, Z. Transients Extraction Based on Averaged Random Orthogonal Matching Pursuit Algorithm for Machinery Fault Diagnosis. *IEEE Trans. Instrum. Meas.* **2017**, *66*, 3237–3248. [CrossRef]

47. El Bouchikhi, E.H.; Choqueuse, V.; Benbouzid, M. Induction machine faults detection using stator current parametric spectral estimation. *Mech. Syst. Signal Process.* **2015**, *52–53*, 447–464. [CrossRef]

48. Avalos, G.; Aguayo, S.; Rangel-Magdaleno, J.; Paternina, M. Bearing fault detection in induction motors using digital Taylor-Fourier transform. In Proceedings of the 2022 International Conference on Electrical Machines (ICEM), Valencia, Spain, 5–8 September 2022; pp. 1830–1835. [CrossRef]

49. Boudinar, A.H.; Benouzza, N.; Bendiabdellah, A.; Khodja, M.-E. Induction Motor Bearing Fault Analysis Using a Root-MUSIC Method. *IEEE Trans. Ind. Appl.* **2016**, *52*, 3851–3860. [CrossRef]

50. Elbouchikhi, E.; Choqueuse, V.; Benbouzid, M. Induction machine bearing faults detection based on a multi-dimensional MUSIC algorithm and maximum likelihood estimation. *ISA Trans.* **2016**, *63*, 413–424. [CrossRef]

51. Xu, S.; Dai, H.; Feng, L.; Chen, H.; Chai, Y.; Zheng, W.X. Fault Estimation for Switched Interconnected Nonlinear Systems with External Disturbances via Variable Weighted Iterative Learning. *IEEE Trans. Circuits Syst. II Express Briefs* **2023**. [CrossRef]

52. Huang, N.; Chen, Q.; Cai, G.; Xu, D.; Zhang, L.; Zhao, W. Fault Diagnosis of Bearing in Wind Turbine Gearbox Under Actual Operating Conditions Driven by Limited Data with Noise Labels. *IEEE Trans. Instrum. Meas.* **2020**, *70*, 1–10. [CrossRef]

53. Xu, B.; Sun, L.; Xu, L.; Xu, G. Improvement of the Hilbert Method via ESPRIT for Detecting Rotor Fault in Induction Motors at Low Slip. *IEEE Trans. Energy Convers.* **2013**, *28*, 225–233. [CrossRef]

54. Liang, X.; Ali, M.Z.; Zhang, H. Induction Motors Fault Diagnosis Using Finite Element Method: A Review. *IEEE Trans. Ind. Appl.* **2019**, *56*, 1205–1217. [CrossRef]

55. Marfoli, A.; Bolognesi, P.; Papini, L.; Gerada, C. Mid-Complexity Circuital Model of Induction Motor with Rotor Cage: A Numerical Resolution. In Proceedings of the 2018 XIII International Conference on Electrical Machines (ICEM), Alexandroupoli, Greece, 3–6 September 2018; IEEE: Piscataway, NJ, USA, 2018; pp. 277–283. [CrossRef]

56. Faiz, J.; Ojaghi, M. Unified winding function approach for dynamic simulation of different kinds of eccentricity faults in cage induction machines. *IET Electr. Power Appl.* **2009**, *3*, 461–470. [CrossRef]

57. Asad, B.; Vaimann, T.; Belahcen, A.; Kallaste, A.; Rassõlkin, A.; Iqbal, M.N. Modified winding function-based model of squirrel cage induction motor for fault diagnostics. *IET Electr. Power Appl.* **2020**, *14*, 1722–1734. [CrossRef]

58. Li, C.; Wang, X.; Liu, F.; Ren, J.; Xing, Z.; Gu, X. Analysis of Permanent Magnet-assisted Synchronous Reluctance Motor Based on Equivalent Reluctance Network Model. *CES Trans. Electr. Mach. Syst.* **2022**, *6*, 135–144. [CrossRef]

59. Shen, M.; Pfister, P.-D.; Tang, C.; Fang, Y. A Hybrid Model of Permanent-Magnet Machines Combining Fourier Analytical Model with Finite Element Method, Taking Magnetic Saturation into Account. *IEEE Trans. Magn.* **2020**, *57*, 1–5. [CrossRef]

60. Asad, B.; Vaimann, T.; Belahcen, A.; Kallaste, A.; Rassõlkin, A.; Iqbal, M. The Cluster Computation-Based Hybrid FEM–Analytical Model of Induction Motor for Fault Diagnostics. *Appl. Sci.* **2020**, *10*, 7572. [CrossRef]

61. Dong, N.; Roychowdhury, J. General-Purpose Nonlinear Model-Order Reduction Using Piecewise-Polynomial Representations. *IEEE Trans. Comput. Des. Integr. Circuits Syst.* **2008**, *27*, 249–264. [CrossRef]

62. Kassis, M.T.; Kabir, M.; Xiao, Y.Q.; Khazaka, R. Passive Reduced Order Macromodeling Based on Loewner Matrix Interpolation. *IEEE Trans. Microw. Theory Tech.* **2016**, *64*, 2423–2432. [CrossRef]

63. Zhai, Y.; Vu-Quoc, L. Analysis of Power Magnetic Components with Nonlinear Static Hysteresis: Proper Orthogonal Decomposition and Model Reduction. *IEEE Trans. Magn.* **2007**, *43*, 1888–1897. [CrossRef]

64. Far, M.F.; Martin, F.; Belahcen, A.; Montier, L.; Henneron, T. Orthogonal Interpolation Method for Order Reduction of a Synchronous Machine Model. *IEEE Trans. Magn.* **2017**, *54*, 1–6. [CrossRef]

65. Bai, Z. Krylov subspace techniques for reduced-order modeling of large-scale dynamical systems. *Appl. Numer. Math.* **2002**, *43*, 9–44. [CrossRef]

66. Huang, S.; Tan, K.K. Fault Simulator Based on a Hardware-in-the-Loop Technique. *IEEE Trans. Syst. Man Cybern. Part C Appl. Rev.* **2012**, *42*, 1135–1139. [CrossRef]

67. Nadarajan, S.; Panda, S.K.; Bhangu, B.; Gupta, A.K. Online Model-Based Condition Monitoring for Brushless Wound-Field Synchronous Generator to Detect and Diagnose Stator Windings Turn-to-Turn Shorts Using Extended Kalman Filter. *IEEE Trans. Ind. Electron.* **2016**, *63*, 3228–3241. [CrossRef]

68. Bachir, S.; Tnani, S.; Trigeassou, J.-C.; Champenois, G. Diagnosis by parameter estimation of stator and rotor faults occurring in induction machines. *IEEE Trans. Ind. Electron.* **2006**, *53*, 963–973. [CrossRef]

69. Zhang, S.; Dong, H.; Maschek, U.; Song, H. A digital-twin-assisted fault diagnosis of railway point machine. In Proceedings of the 2021 IEEE 1st International Conference on Digital Twins and Parallel Intelligence (DTPI), IEEE, DTPI, Beijing, China, 15 July–15 August 2021; pp. 430–433. [CrossRef]

70. Bui, V.P.; Chadebec, O.; Rouve, L.-L.; Coulomb, J.-L. Noninvasive Fault Monitoring of Electrical Machines by Solving the Steady-State Magnetic Inverse Problem. *IEEE Trans. Magn.* **2008**, *44*, 1050–1053. [CrossRef]

71. Huang, Y.; Zhao, M.; Zhang, J.; Lu, M. The Hall Sensors Fault-Tolerant for PMSM Based on Switching Sensorless Control with PI Parameters Optimization. *IEEE Access* **2022**, *10*, 114048–114059. [CrossRef]

72. Zarch, M.G.; Alipouri, Y.; Poshtan, J. Fault Detection Based on Online Probability Density Function Estimation. *Asian J. Control.* **2016**, *18*, 2193–2202. [CrossRef]

73. Guo, J.; Queval, L.; Roucaries, B.; Vido, L.; Liu, L.; Trillaud, F.; Berriaud, C. Nonlinear Current Sheet Model of Electrical Machines. *IEEE Trans. Magn.* **2019**, *56*, 1–4. [CrossRef]

74. Frosini, L.; Harlisca, C.; Szabo, L. Induction Machine Bearing Fault Detection by Means of Statistical Processing of the Stray Flux Measurement. *IEEE Trans. Ind. Electron.* **2014**, *62*, 1846–1854. [CrossRef]

75. Lang, W.; Hu, Y.; Gong, C.; Zhang, X.; Xu, H.; Deng, J. Artificial Intelligence-Based Technique for Fault Detection and Diagnosis of EV Motors: A Review. *IEEE Trans. Transp. Electrif.* **2021**, *8*, 384–406. [CrossRef]

76. Wu, M.; Chen, D.; Chen, G. New Spectral Leakage-Removing Method for Spectral Testing of Approximate Sinusoidal Signals. *IEEE Trans. Instrum. Meas.* **2012**, *61*, 1296–1306. [CrossRef]